

Provided for non-commercial research and education use.
Not for reproduction, distribution or commercial use.



(This is a sample cover image for this issue. The actual cover is not yet available at this time.)

This article appeared in a journal published by Elsevier. The attached copy is furnished to the author for internal non-commercial research and education use, including for instruction at the authors institution and sharing with colleagues.

Other uses, including reproduction and distribution, or selling or licensing copies, or posting to personal, institutional or third party websites are prohibited.

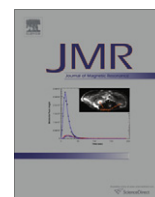
In most cases authors are permitted to post their version of the article (e.g. in Word or Tex form) to their personal website or institutional repository. Authors requiring further information regarding Elsevier's archiving and manuscript policies are encouraged to visit:

<http://www.elsevier.com/copyright>



Contents lists available at SciVerse ScienceDirect

Journal of Magnetic Resonance

journal homepage: www.elsevier.com/locate/jmrSingle bead detection with an NMR microcapillary probe [☆]Yoshihiro Nakashima ^{a,b,*}, Michael Boss ^a, Stephen E. Russek ^a, John Moreland ^a^a National Institute of Standards and Technology, Boulder, CO 80305, USA^b Kyushu University, Fukuoka, Japan

ARTICLE INFO

Article history:

Received 2 March 2012

Revised 1 September 2012

Available online 15 September 2012

Keywords:

Magnetic particle
Single particle detection
Microcoil NMR
MRI contrast agent

ABSTRACT

We have developed a nuclear magnetic resonance (NMR) microcapillary probe for the detection of single magnetic microbeads. The geometry of the probe has been optimized so that the signal from the background water has a similar magnitude compared to the signal from the dephased water nearby a single magnetic bead within the probe detector coil. In addition, the RF field of the coil must be uniform within the effective range of the magnetic bead. Three different RF probes were tested in a 7 T (300 MHz) pulsed NMR spectrometer with sample volumes ranging from 5 nL down to 1 nL. The 1 nL probe had a single-shot signal-to-noise ratio (SNR) for pure water of 27 and a volume resolution that exhibits a 600-fold improvement over a conventional (5 mm tube) NMR probe with a sample volume of 18 μ L. This allowed for the detection of a 1 μ m magnetite/polystyrene bead ($m = 2 \times 10^{-14}$ A m²) with an estimated experimental SNR of 30. Simulations of the NMR spectra for the different coil geometries and positions of the bead within the coil were developed that include the B_0 shift near a single bead, the inhomogeneity of the coils, the local coil sensitivity, the skin effect of the coil conductor, and quantitated estimates of the proximity effect between coil windings.

Published by Elsevier Inc.

1. Introduction

Iron oxide particles have a strong effect on the transverse relaxation time (T_2^*) of nearby water protons and thus are useful as magnetic resonance imaging (MRI) contrast agents [1]. Single cell [2] and single magnetic particle detection [3] have been demonstrated via MRI, but quantitative measurements are limited by the image voxel dimensions and the precise location of the particle within the voxel. Microcoil NMR spectroscopy has the potential to further characterize the details of the NMR signature of isolated magnetic particles in water, but improving upon state-of-the-art probe designs is necessary.

Sillerud et al. have shown that concentrations as low as 10 beads/nL of 1 μ m magnetic beads can be detected by ¹H NMR at 1 T in a 264 nL sample [4] by measuring frequency shifts and line broadening. Single particle detection, on the other hand, requires a specialized NMR probe, one capable of detecting the difference between background water and water within the range of influence of the bead. In this paper, we present an NMR probe for single bead detection that is based on the pioneering work of Olson et al. [5]. We numerically analyze the magnetic field around

a single bead to estimate the volume of water affected by a single bead as well as the distribution of the B_0 field within that volume. The RF uniformity as a function of the number of turns of the microcoil is calculated to determine an optimum configuration. Simulated NMR spectra for the different RF coil geometries and bead positions are also calculated. Three different probes were fabricated and tested with sample volumes ranging from 5 nL down to 1 nL.

2. Probe design

The NMR spectrometer signal-to-noise ratio (SNR) is fundamentally limited by the RF coil characteristics. Hoult and Richards report a general expression for SNR [6], and Peck et al. have adopted it specifically for microcoil NMR [7], finding that:

$$\text{SNR} = K\omega_0^2(B_1/i)(k_0 v_{\text{sample}}/V_{\text{noise}}). \quad (1)$$

Here $K = N\gamma\hbar^2 I(I+1)/3\sqrt{2}k_B T_s$, where N is the spin density, γ is the gyromagnetic ratio, \hbar is reduced Planck's constant, I is spin quantum number, k_B is Boltzmann's constant, T_s is temperature of sample, and k_0 is a scaling constant to account for the RF inhomogeneity of the B_1 field. V_{noise} is the electrical noise associated with the NMR detection circuit, which is mainly the Johnson noise of the RF coil. $V_{\text{noise}} = \sqrt{4k_B T_c R \Delta f}$, where T_c is the temperature of the coil and R is its resistance, and Δf is the measurement spectral bandwidth. More importantly, we see that the SNR is proportional to the sample volume, v_{sample} . For single bead detection, v_{sample} is

[☆] Contribution of the National Institute of Standards and Technology, not subject to copyright.

* Corresponding author. Address: NIST Mail Stop 687.03, 325 Broadway, Boulder, CO 80305-3328, USA. Fax: +1 303 497 3725.

E-mail address: yoshihiro.nakashima@nist.gov (Y. Nakashima).

separated into two volumes: the background fluid volume, v_{back} , and the volume of the fluid affected by a single bead, v_{aff} . When v_{aff} is relatively small compared to v_{back} , the spectrum shape is dominated by the background signal. Furthermore, by definition, if v_{aff} is smaller than v_{sample}/SNR , the NMR signal from v_{aff} will be buried in the noise. In short, v_{sample}/SNR determines the detection limit volume for an $SNR = 1$. To maximize the NMR signal for single bead detection, we need to increase the RF strength per unit current (B_1/i) for better volume resolution. Thus, a microcoil is appropriate for detecting beads a few micrometers in size. We numerically calculate the B_0 field distortion, ΔB_0 , as well as the microscopic inhomogeneity in the B_1 field to better optimize the NMR probe design.

We estimate the magnetic moment of a uniformly magnetized 1 μm diameter polystyrene bead to be $m = 2.3 \times 10^{-14} \text{ A m}^2$, based on a saturation magnetization of $4.3 \times 10^4 \text{ A/m}$, as provided by the manufacturer. Given these values, the ΔB_0 field contours near the bead can be determined by calculation. The results are shown in Fig. 1a. They define the effective range of a bead for significant shifts in the proton Larmor frequency within the bandwidth of the spectrometer. Shifts of at least 10 Hz are observed within a 50 μm region surrounding the bead; shifts of at least 1 Hz are observed within a 120 μm region; and shifts of at least 0.1 Hz are observed within a 250 μm region.

To investigate the influence of v_{sample} on the NMR spectrum, we calculated the magnetic field at each grid point (grid size is $0.5 \times 0.5 \times 0.5 \mu\text{m}$) and generated a histogram of the number of volume elements as a function of ΔB_0 within the capillary. The histograms are shown in Fig. 2. Note that the sample volume is defined by the capillary ID, and the effective length of the coil (l_s) ranging from 100 μm to 1000 μm along the axis of the capillary, which correspond to v_{sample} ranges from 0.5 nL to 5 nL. Due to the orientation of the capillary (transverse to B_0), the effect of the negative B_0 shift region (as shown in Fig. 2) will dominate the NMR spectra. The influence of the bead on the NMR spectrum as it passes through the coil can be increased by changing either the capillary ID or the magnetic moment of the particle. In particular we have used the 0.1 Hz shift (hatched region shown in Fig. 2) as

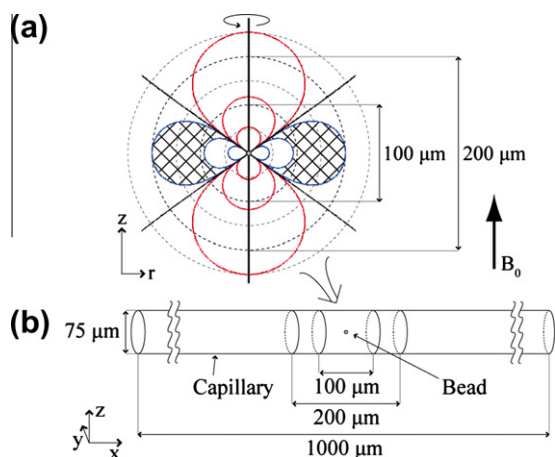


Fig. 1. Calculated ΔB_0 shift near a magnetic bead. (a) ΔB_0 field shifts of a 1 μm sphere having magnetization of $4.3 \times 10^4 \text{ A/m}$ in a 7 T uniform magnetic field. Contour lines show a ΔB_0 of $\pm 230 \text{ nT}$, $\pm 23 \text{ nT}$ and $\pm 2.3 \text{ nT}$, corresponding to shift of 10 Hz, 1 Hz, and 0.1 Hz in the proton Larmor frequency. Red lines indicate a positive magnetic field, blue lines indicate a negative magnetic field, and black lines indicate $\Delta B_0 = 0$. The hatched area shows the region around the bead having a 0.1–1 Hz shift that just fits into the ID of the capillary. (b) Schematic view of volume used in the simulations to develop the ΔB_0 histograms. A magnetized 1 μm sphere is placed on the center of the sample volume; v_{sample} is limited by the 75 μm ID of the capillary and the length of the sample ranging 100 μm to 1000 μm . This corresponds to a v_{sample} of 0.5–5 nL. (For interpretation of the references to colour in this figure legend, the reader is referred to the web version of this article.)

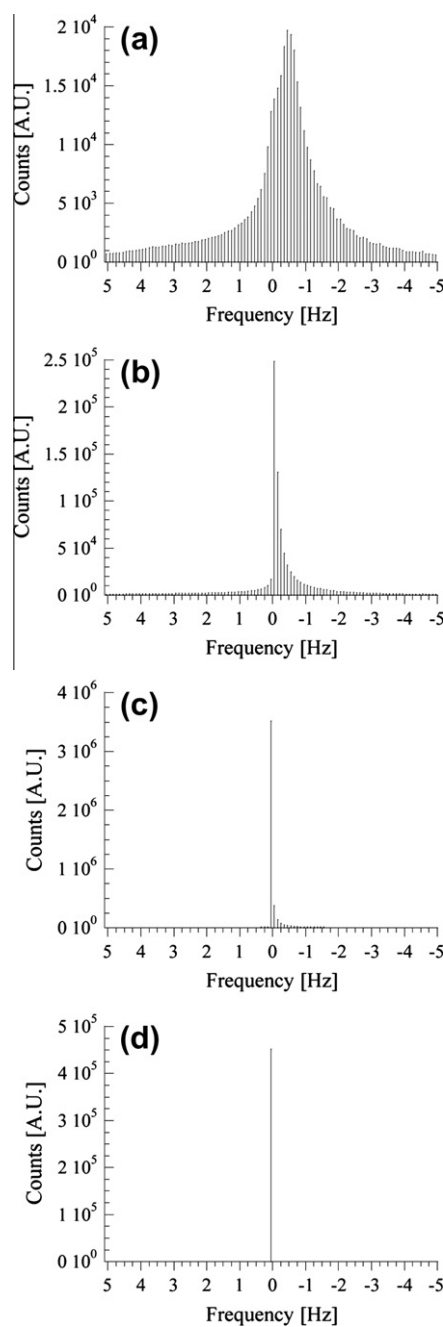


Fig. 2. ΔB_0 histograms near a magnetic bead in the capillary as a function of l_s . (a) 100 μm , (b) 200 μm and (c) 1000 μm . (d) ΔB_0 histogram without the presence of a magnetic bead. If a bead is not in the sample, we would see only one peak as shown. Note that for all of the histograms, a shift of $\pm 5 \text{ Hz}$ in the proton Larmor frequency corresponds to $\pm 115 \text{ nT}$ of ΔB_0 , and the step size is 0.1 Hz.

a primary design criterion for optimizing the coil geometry. The spread in ΔB_0 is most obvious for the $l_s = 100 \mu\text{m}$, with a corresponding peak shift to -0.5 Hz and significant broadening. The peak height becomes 4% of that of the ΔB_0 distribution for pure water because the large frequency shift of water protons in the neighborhood of a bead causes significant line broadening. The ΔB_0 distribution for $l_s = 200 \mu\text{m}$ had a 12-fold higher peak than that for $l_s = 100 \mu\text{m}$, as well as a peak shift of -0.1 Hz and broadening. Note that the ΔB_0 distribution for the $l_s = 200 \mu\text{m}$ is virtually the same as the $l_s = 100 \mu\text{m}$ outside of the frequency range of -0.1 Hz to -0.7 Hz . However, there are significantly more spins inside this range for the $l_s = 200 \mu\text{m}$ sample owing to additional spins

that are farther from the bead, which are less affected than the spins in its immediate vicinity. When v_{eff} and v_{sample} are approximately equal, the peak distortion can easily be observed. In this case the v_{sample} just encompasses the cross-hatched region in Fig. 1a. On the other hand, for sample volumes greater than 1 nL ($l_s \geq 200 \mu\text{m}$), v_{back} will dominate the histogram. The histogram for the largest sample volume ($l_s = 1000 \mu\text{m}$) shows a narrow ΔB_0 distribution indicating that the majority of spins in the sample remained unaffected by the bead, as expected. For comparison, the ΔB_0 distribution without beads for the $l_s = 100 \mu\text{m}$ is also shown in Fig. 2d.

The minimum detectable sample volume is determined by the probe SNR limitations, as discussed above. However, since one of the goals of this research is to develop new methods for quantitative measurements of the magnetic moment of single bead, it is important to have a large enough v_{sample} to capture the details of the ΔB_0 distribution. According to this analysis, we estimate the minimum v_{sample} required to realistically detect a single bead to be 1 nL. In this case, the signal strength is large and the spectrum broadening can be detected. This leads to the conclusion that the NMR RF coil must have a small sample volume, but the volume must also be large enough to cover the effective range of a single magnetic bead for better SNR.

The skin effect of the coil conductor and the proximity effect between the coils make it difficult to calculate the detailed characteristics of the RF coils [7,8]. For this reason we developed an FEM analysis for the B_1 inhomogeneity which includes both skin effects and proximity effects for different coil lengths. The FEM analysis was based on a two-dimensional, axis symmetric model at 300 MHz. B_1 inhomogeneity plots for 4-, 8-, and 17-turn RF coils, corresponding to l_s of 240, 490, and 1100 μm and v_{sample} of 1, 2, and 5 nL within the coil region, are shown in Fig. 3. RF uniformity on the x -axis is given $B_1(x)/B_1(0)$, where $B_1(x)$ is the B_1 field produced by the RF coil along the x -axis and $B_1(0)$ is the B_1 field at the center of the coil. Smaller coils have less RF uniformity. However, B_1 distribution in the transverse direction is relatively homogenous in the sample region. In this case the B_1 homogeneity of the sample region is determined by the RF uniformity on the x -axis direction. With the 4-turn coil, the B_0 distortion range of the bead in the sample volume mostly fits into the 10% error range. With the 8-turn coil, the B_0 distortion range is covered in the 5% error range. With the 17-turn coil, the B_0 distortion range is fully covered in the 1% error range for the B_1 uniformity. Other coil characteristics such as resistance of the coil and B_1/i are also calculated with FEM. Results are shown in Fig. 4.

Based on the calculations described above, we can numerically simulate NMR spectra by convolving the ΔB_0 histograms and the natural proton line spectrum with B_1 uniformity of coils as follows:

$$S_{\text{NMR}} = \frac{L(f) * \delta_{\text{RF}}(V)}{V_{\text{noise}}}, \quad (2)$$

where $F(f)$ is a natural proton line spectrum given as a Lorentzian function, $\delta_{\text{RF}}(V)$ is a ΔB_0 shift distribution of the induced NMR signal from the sample after a 90° pulse given as a delta function. We divided a sample region into a series of disks, $V_{x_k} = S_s(x_{k+1} - x_k)$ along the x -axis, where S_s is the cross section of the sample. Assuming that the RF homogeneity in transverse direction $B_1(x_k)$ is constant within each discrete disk volume, $\delta_{\text{RF}}(V)$ is given by:

$$\delta_{\text{RF}}(V) = \sum_{k=0}^{\infty} \left\{ \delta(V_{x_k}) \varphi(x_k) \sin\left(\theta + \frac{\pi}{2} \frac{B_1(x_k)}{B_1(0)}\right) \right\} \quad (3)$$

$\delta(V_{x_k})$ is the ΔB_0 shift distribution of unit sample volume of V_{x_k} given as delta function, and $\varphi(x_k)$ is the magnetic flux which penetrates the RF coil induced by a magnetic dipole m at the point x_k . Note the following: (1) $\varphi(x) \propto B_1(x)$ by reciprocity, and

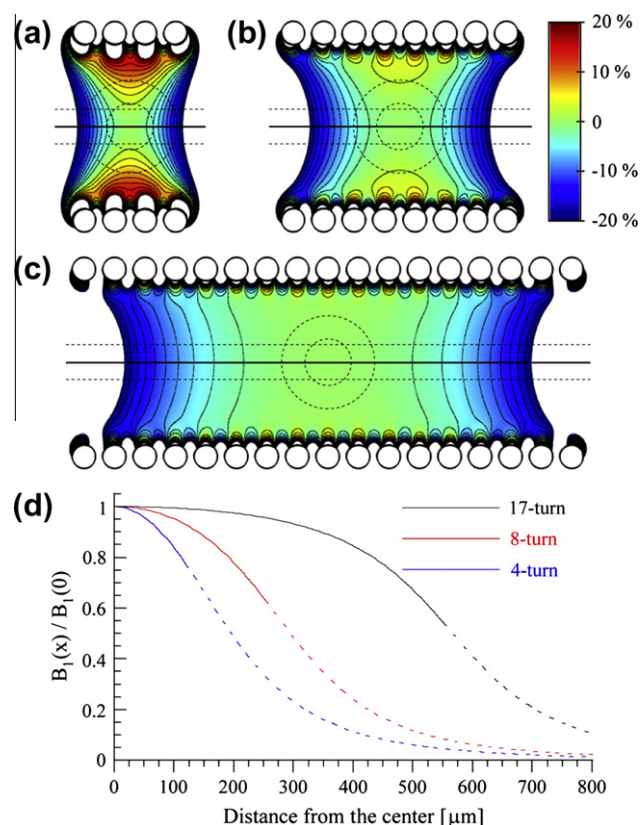


Fig. 3. RF homogeneity based on FEM analysis for the different coil geometries at 300 MHz: (a) 4-turn coil, (b) 8-turn coil and (c) 17-turn coil. Contour lines show a $\pm 2\%$ error in B_1 uniformity from the center of the RF coil. The circle in the center shows an estimated bead effective range diameter of 100–200 μm . The broken line shows the sample volume defined by a 75 μm ID capillary. Due to the cylindrical symmetry of the problem, a number of loop coils (diameter of 420 μm with 50 μm conductor) were used assuming a continuous multi-turn coil. The horizontal axis in the center is the symmetric axis. (d) RF homogeneity along the axis. Solid lines show inside of the coil regions and broken lines show outside of the coil regions.

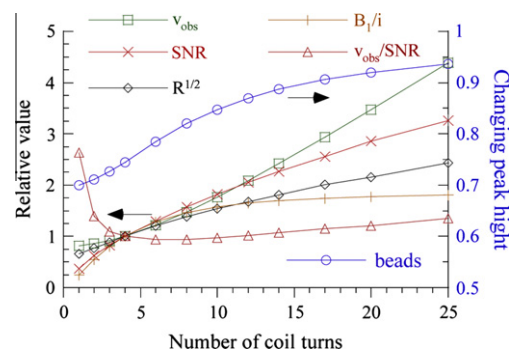


Fig. 4. RF coil characteristics as a function of the number of coil turns. The B_1 inhomogeneity of the coils and the local coil sensitivity are used to define the observable volume of the coil v_{obs} . FEM analysis that includes both the skin effect and the proximity effect is used to determine the coil sensitivity B_1/i as well as the RF resistance R . These values are then used to determine total SNR. v_{obs} , SNR, root (R), B_1/i , and $v_{\text{obs}}/\text{SNR}$ are plotted here normalized by values for the 4-turn coil. The 4-turn coil characteristics are $v_{\text{obs}} = 1.5 \text{ nL}$, $B_1/i = 1.5 \times 10^{-3} \text{ T/A}$, and $R = 0.37 \Omega$. Right axis shows the expected NMR peak height difference with and without a bead in the coil as a function of the number of coil turns.

$\sin\left(\theta + \frac{\pi}{2} \frac{B_1(x_k)}{B_1(0)}\right)$ is the tipping angle of the dipole at the point x_k after a 90° pulse. The effect of a bead in the coil is maximized at $\theta = 0$. (2) B_1 falls off at the end of the coils as shown in Fig. 3. Even so, protons

more than 150 μm from the end of the coil would be excited. (3) A generic scaling constant k_0 has been used in the past to consider the effect of RF inhomogeneities on the NMR response of microcoil probes. However, if we know the RF inhomogeneity, the observable sample volume ($v_{obs} = k_0 v_{sample}$) is given by:

$$v_{obs} = \int \left\{ S_s \frac{B_1(x)}{B_1(0)} \sin\left(\theta + \frac{\pi B_1(x)}{2 B_1(0)}\right) \right\} dx. \quad (4)$$

The theoretical estimates of coil SNR and v_{obs} are shown in Fig. 4. The B_1 inhomogeneity of the coils, the local coil sensitivity, and the coil resistance including both skin effect and proximity effects have been used in the SNR calculation as discussed above.

Simulated NMR spectra are shown in Fig. 5. With a 17-turn coil, the peak height difference with and without beads is only 10%, and it is difficult to see the effect of a bead from the spectrum. With a 4-turn coil, the peak height drops by 25%, and the peak width increases to 0.9 Hz from 0.7 Hz and the peak shifts to -0.1 Hz. Peak reduction is an indication of the volume of affected spins, and the peak broadening is a measure of the ΔB_0 distribution within that volume. In principle, these parameters can be used to determine the magnetic moment of the bead. The direction of the peak shift

indicates the majority of the ΔB_0 distribution within that volume is either positive or negative. Note that peak shift alone would not be good way to estimate the effect of the magnetic moment of the bead. A larger RF coil has better SNR, however smaller RF coils have a smaller v_{aff}/v_{sample} ratio, and therefore are more sensitive to the influence of a single bead. Note that, one may think that a 1- or 2-turn coil having a high v_{aff}/v_{sample} ratio would be better for single bead detection, but the low SNR makes the detection limit volume smaller as shown in Fig. 4. Therefore one needs to select the proper number of RF coil turns to be from 3- to 15-turns, given the effective range of magnetic bead.

Moreover, the bead position in the sample region influences the NMR spectra, especially for smaller coils. The simulated NMR spectra for a 4-turn RF coil as a function of bead position along the x -, y -, and z -axis is shown in Fig. 6. In the transverse direction, the bead position has a small effect on the NMR spectra, except for the peak shift. Along the z -axis, peak shift reduces to 0. At this point the ΔB_0 distribution polarity in the sample region moves from the negative side to the neutral. In contrast, the inhomogeneity of the RF field along x -axis causes significant spectral changes as a function of bead position.

3. Experimental setup

We fabricated three different NMR microfluidic capillary probes for use in a commercial pulsed NMR spectrometer operating at 7 T (300 MHz). The microcoil NMR probe design is based on that described by Olson et al. [5] with modifications based on the FEM results described above. A detailed schematic of the probe assembly is shown in Fig. 7. 17-, 8- and 4-turn coils were made from 50 μm diameter copper wire with varnish insulation. Microcoils were

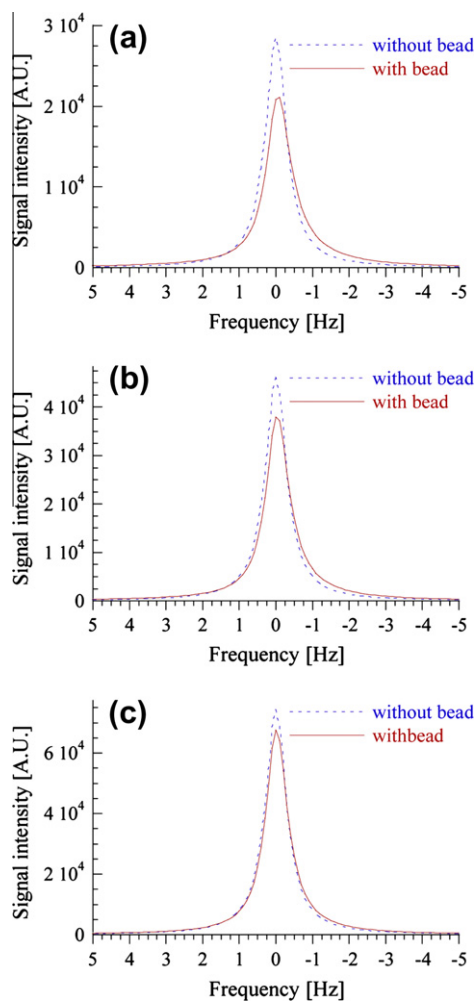


Fig. 5. Simulated NMR spectra with (red) and without (blue) the presence of single magnetic bead. (a) 4-turn coil – the spectra width broadened 0.2 Hz, peak shifts -0.08 Hz, and peak height reduced 25% with the presence of bead. (b) 8-turn coil – the spectra width broadened 0.1 Hz, peak shifts -0.05 Hz, and peak height reduced 18% with the presence of bead. (c) 17-turn coil – the spectra width broadened 0.06 Hz, peak shifts -0.02 Hz, and peak height reduced 9% with the presence of bead. (For interpretation of the references to colour in this figure legend, the reader is referred to the web version of this article.)

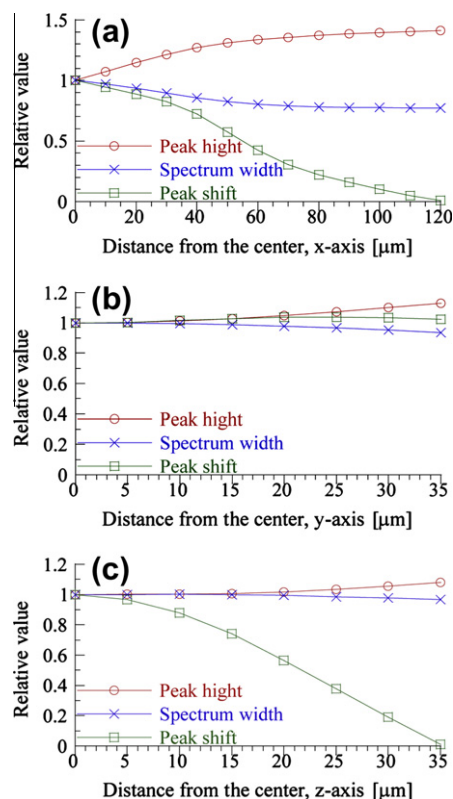


Fig. 6. Calculated values for the spectrum parameters including peak height, width, and shift as a function of the bead position within the 4-turn coil: (a) along the x -axis, (b) along the y -axis, and (c) along the z -axis. Each value is normalized with to the values at the center of the coil.

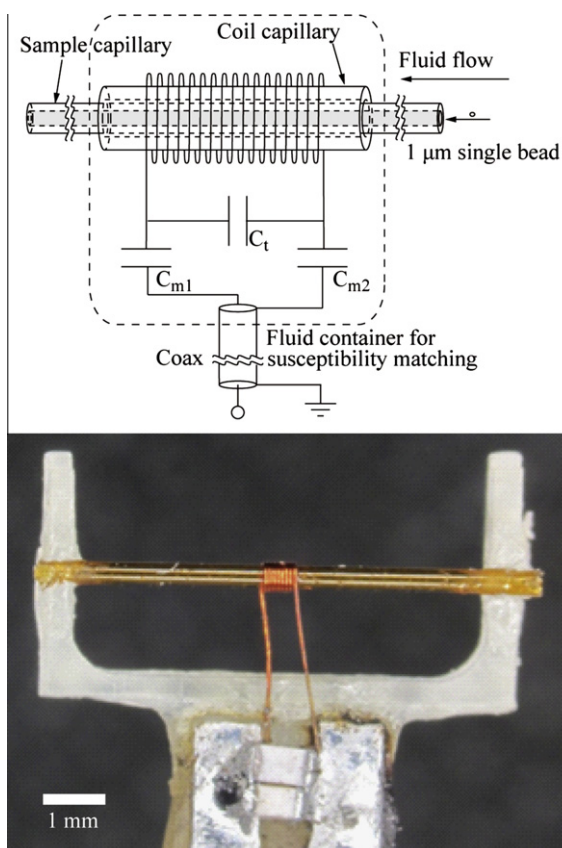


Fig. 7. Schematic diagram and picture of microcoil NMR probe. The microcoil was wound on a “coil capillary” with an inner, removable, “sample capillary.” The RF coil and tuning/matching capacitors were immersed in a perfluorinated susceptibility-matching fluid.

wrapped around fused silica capillaries having a 350 μm OD and 180 μm ID. The coil leads were soldered to a printed circuit board (PCB), modified to eliminate as much material as possible in order to reduce the susceptibility effects of the PCB fiber epoxy. Non-magnetic chip capacitors were also placed on the PCB to both tune the coil to 300 MHz and impedance match to the 50 Ω transmission line. The unit was connected to the NMR preamplifier by a nonmagnetic rigid coaxial cable. A “sample capillary” (fused silica, OD = 150 μm , ID = 75 μm) was mounted through the “coil capillary”. In this way, the coil capillary could be reused if debris were to become lodged in the sample capillary. To reduce B_0 inhomogeneities, due to differences in the magnetic susceptibility of the probe components surrounding the sample, including the capillaries, coil, and air gaps between the capillaries, we immersed the PCB into a perfluorinated hydrocarbon liquid, which has a magnetic susceptibility similar to that of copper [5]. The probe was immersed in a 25 mL glass bottle. Samples were injected into the sample capillary with a syringe pump. Coil lengths and sample volumes are shown in 10 mm Table 1.

Table 1
Characteristics of the NMR probe.

Coil turns	Coil length	Sample volume (v_{sample})	Observable sample volume (v_{obs})	SNR	Detection limit (nL) ($v_{\text{obs}}/\text{SNR}$)	Spectrum resolution
17-turn	1100 μm	4.8 nL	4.7 nL	71	0.07	0.7 Hz
8-turn	490 μm	2.2 nL	2.4 nL	38	0.06	0.7 Hz
4-turn	240 μm	1.1 nL	1.6 nL	27	0.06	0.6 Hz
5 mm NMR with 2 mm capillary	–	18 μL	18 μL	480	38	0.7 Hz

Sample solutions consisted of 1 μm polystyrene beads with embedded iron oxide nanoparticles (26% iron by weight) dispersed in water [9]. To achieve a concentration of a single bead per coil volume, the stock solution was diluted with deionized water to 3×10^4 beads/mL or 1 bead per 30 nL. Bead concentrations were experimentally verified with an optical hemocytometer after dilution.

4. Measurements

All experiments were conducted at 7.05 T ($f_0 = 300.18$ MHz). Each probe was shimmed *in situ* with the shim coils of the spectrometer. Experiments were performed on pure de-ionized (DI) water without flow and on bead solutions. The water measurements were used to determine the baseline SNR and spectrum resolution. We also compared the characteristics of the microcoil probes with a conventional 5 mm commercial probe and a 2 mm sample tube. The spectral width for pure DI water samples was between 0.6 Hz and 0.7 Hz for all of the coils tested. Occasionally, we observed effects brought on by the susceptibility mismatches in the multilayered capillary geometry that made it difficult to reproduce spectral line widths of 0.6 Hz for pure water. For this reason, shimming target values were set to 1 Hz for practical use.

Measurements on bead solutions were made in the following way. First, we stepped the motor of the syringe pump one step (1.4 nL), then waited 60 s for the flow rate to decrease to 10 pL/s, corresponding to a bead velocity of 2 $\mu\text{m}/\text{s}$. We then measured the free induction decay (FID) four times. The 90° pulse widths were between 19 μs and 23 μs . Each FID measurement took 16.5 s (5 T_1 for pure water). The measurement sequence is shown in Fig. 8. It was difficult to predict when a bead would pass into the sample region of the probe, so we repeated this sequence as individual beads would occasionally enter the coil region of the capillary. We found that repeating the sequence 100 times was sufficient to see the signals from several beads as they passed through the coil. As a control and to check the stability of the experiment, DI water was measured with the same sequence in advance. During the sample flow experiments, measurements were stable. We could not see the effect of pumping or flow induced line broadening. A D_2O lock was not used. The drift rate was less than 6.6 mHz/s (0.14 nT/s), which was acceptable for the 15 s FID measurement period. Peak shift measurements were renormalized between each FID measurement to accommodate field drift.

5. Results

The SNR and the spectral resolution for pure DI water are shown in Table 1 for different coil geometries. The SNR for the microcoils was 6–14% of that of the conventional 5 mm tube NMR probe with a much larger sample volume. However the detection limit volume improved more than 600-fold for the 4-turn microcoil probe, compared to the 5 mm commercial probe.

We would observe a series of momentary anomalous spectra as a single bead moved through the coil during the flow experiments. The line shape of the anomalous spectra varied, which is to be

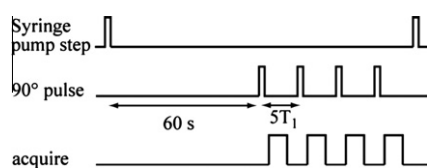


Fig. 8. Measurement sequence: (1) the syringe pump steps 1.4 nL of sample into the capillary; (2) 60 s delay for flow to stabilize; (3) 4 FID signals were measured using a 90° pulse; (4) sequence repeated 100 times. 400 FID signals were acquired for each measurement.

expected depending on the position of the bead within the NMR coil. A peak that was more than 2% lower than that for DI water was considered a signal for the presence of a bead in the coil. Sometimes the spectrum would become fixed after several FID measurements. We think this was due to a single bead sticking to the inner wall of the capillary. NMR spectra from three different probes are shown in Fig. 9. The presence of a bead in the coil lowered the peak height, broadened the peak, and shifted it to lower frequency. With the 17-turn coil, only the first 85 signals were

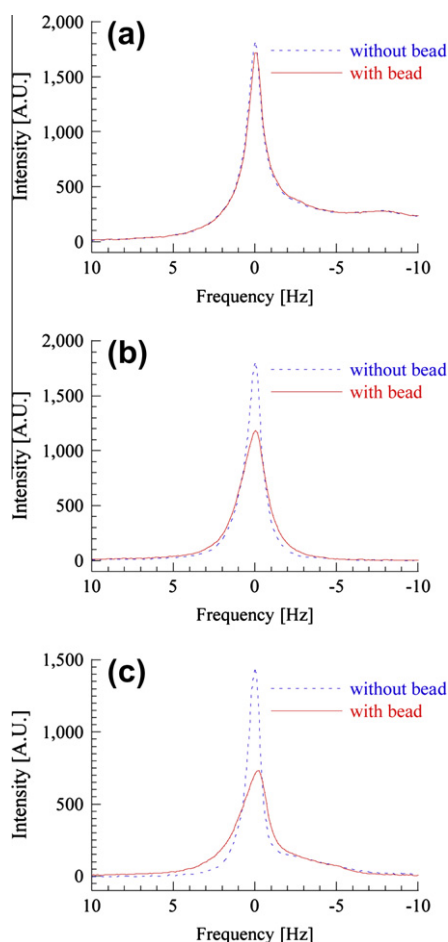


Fig. 9. Spectra of DI water with (blue) and without (black) the presence of single magnetic bead. (a) Signal from 17-turn microcoil – the spectral width of pure water is 1.1 Hz compared to 1.2 Hz with the presence of bead. (b) Signal from 8-turn microcoil – the spectral width of pure water is 1.0 Hz compared to 1.8 Hz with the presence of a bead. (c) Signal from 4-turn microcoil – the spectral width of pure water alone is 1.0 Hz compared to 2.2 Hz with the presence of a bead. Pulse sequence conditions: One scan, spectral width ± 1953 Hz, 32768 data points, a 90° pulse width of 19 μ s in (a), 21 μ s in (b), and 23 μ s in (c). (For interpretation of the references to colour in this figure legend, the reader is referred to the web version of this article.)

analyzed. After 85 pulse sequences, a bead lodged in the capillary as discussed above. A total of 17 of 85 sequences indicated the transition of a bead through the coil. A representative spectrum in Fig. 9a shows only a 7% lower spectrum peak and detecting the differences between spectra, with and without a bead, was difficult. With the 8-turn coil, 74 of 400 signals indicated the transition of a bead. A representative spectrum in Fig. 9b shows a peak reduction of 34% and a peak broadening ranging from 1 Hz to 1.8 Hz. With the 4-turn coil, again a bead lodged in the capillary after 116 signals, of which 19 signals indicated the transition of a bead. A representative spectrum in Fig. 9c shows a 50% peak reduction, peak broadening ranging from 1 Hz to 2.2 Hz, and a shift of -0.2 Hz. In this case T_2^* was reduced by two thirds from 320 ms to 140 ms.

6. Discussion

Experimentally we observed that the effect of a bead in a coil is substantially larger than expected based on our simulations. The magnetization of the bead would have to be four-times larger than our original estimate given the experimentally observed peak height reduction, and 20-times larger given the observed spectral broadening. The discrepancies between the experimental and simulated results may be due to several factors. There the possibility that there is a residual inhomogeneity of the B_0 field even after the shimming procedure before making measurements. The simulations for the NMR spectra over estimates the peak height if the residual B_0 inhomogeneity is not accounted for. Thus, the effect of the beads would be less than what would be measured experimentally. Water diffusion may also be important in that the relaxation of spins in an inhomogeneous magnetic field [10] has to be considered. The field gradients near a magnetic bead are large and cause significant non-uniform dephasing of the protons as they pass nearby, which results in spectrum additional broadening. Finally, in our comparisons between theory and experiment we have assumed the bead is located at the center of the coil. The position of the bead within the coil gives rise to different ΔB_0 distributions within the sample volume (as shown in Fig. 6) and so the challenge would be to precisely determine the position of the bead as it travels through the coil for quantitative estimates of the magnetic moment of the bead. At these small scales the flow through the capillary is laminar, so we at least know that its trajectory follows a line parallel to the axis of the coil. A series of spectra taken as the particle traverses the coil could therefore be used to uniquely determine its magnetic moment and position as a function of time.

7. Summary

We have developed a microcapillary NMR probe for detection of a single magnetic bead. The RF coil geometry was optimized to focus on a “limited-volume” sample that cuts off the background signal. The detection limit volume was enhanced 600-fold compared to a conventional 5 mm NMR probe. With the improved sensitivity we were able to measure significant changes in the NMR proton spectrum as a single magnetic bead passed through the coil. Simulations of the NMR spectra for different coil geometries were developed in order to find the optimum probe geometry for detection a single bead with a given magnetic moment. The simulations included calculations of the B_0 shift near a single bead, the B_1 inhomogeneity of the coil, the local coil sensitivity, the skin effect of the coil conductor, and quantitate estimates of the proximity effect between coil windings. The models are useful for probe design for single beads detection but are not as of yet adequate for quantitate measurements of the magnetic moment of a single bead.

Future work will focus on development of new pulse sequences and measurement protocols including gradients to detect the position of the beads in the coil. We plan to also develop more accurate models that include microscopic diffusion effects near the beads. Our goals include using microcoil probes to determine particle aggregation, the distribution of properties such as size and magnetic moments of particles within an ensemble, as well as provide deeper understanding of the relaxation mechanisms of surrounding water protons [11].

Acknowledgments

The authors gratefully acknowledge Gary Zabow and Robert Usselman for their helpful suggestions and discussions. We would also like to thank Anthony Kos for technical support.

References

- [1] J.W.M. Bulte, D.L. Kraitchman, Iron oxide MR contrast agents for molecular and cellular imaging, *NMR Biomed.* 17 (2004) 484–499.
- [2] S.J. Dodd, M. Williams, J.P. Suhan, D.S. Williams, A.P. Koretsky, C. Ho, Detection of single mammalian cells by high-resolution magnetic resonance imaging, *Biophys. J.* 76 (1999) 103–109.
- [3] E.M. Shapiro, S. Skrtic, K. Sharer, J.M. Hill, C.E. Dunbar, A.P. Koretsky, MRI detection of single particles for cellular imaging, *Proc. Natl. Acad. Sci. USA* 101 (2004) 10901–10906.
- [4] L.O. Sillerud, A.F. McDowell, N.L. Adolphi, R.E. Serda, D.P. Adams, M.J. Vasile, T.M. Alam, H-1-NMR detection of superparamagnetic nanoparticles at 1 T using a microcoil and novel tuning circuit, *J. Magn. Reson.* 181 (2006) 181–190.
- [5] D.L. Olson, T.L. Peck, A.G. Webb, R.L. Magin, J.V. Sweedler, High-resolution microcoil H-1-NMR for mass-limited, nanoliter-volume samples, *Science* 270 (1995) 1967–1970.
- [6] D.I. Hoult, R.E. Richards, The signal-to-noise ratio of nuclear magnetic resonance experiment, *J. Magn. Reson.* 24 (1976) 71–85.
- [7] T.L. Peck, R.L. Magin, P.C. Lauterbur, Design and analysis microcoils for NMR microscopy, *J. Magn. Reson. Ser. B* 108 (1995) 114–124.
- [8] K.R. Minard, R.A. Wind, Solenoidal microcoil design. Part II: Optimizing winding parameters for maximum signal-to-noise performance, *Concepts Magn. Res.* 13 (2001) 190–210.
- [9] Dynabeads MyOne SYLANE. Any mention of commercial products does not imply recommendation or endorsement by NIST.
- [10] H.Y. Carr, E.M. Purcell, Effects of diffusion on free precession in nuclear magnetic resonance experiments, *Phys. Rev.* 94 (1954) 630–638.
- [11] G. Zabow, S.J. Dodd, E. Shapiro, J. Moreland, A.P. Koretsky, Microfabricated high-moment micrometer-sized MRI contrast agents, *Magn. Reson. Med.* 65 (2011) 645–655.